Electronic Supplementary Material (ESI) for Materials Chemistry Frontiers.

Electronic Supplementary Information (ESI) for

Fluorophore core-engineered supramolecular discotic columnar liquid crystals with tunable fluorescent behavior

Bin Mu, Xuhong Quan, Yu Zhao, Xun Li and Wei Tian*

Table of Contents

1. Materials and Measurements

Materials

1,3,5-Benzenetricarboxylic acid (>98%, TCI), Ethylenediamine monohydrate (98%, TCI), 1,2-Phenylenediamine (>98%, TCI), 2,3-Diaminonaphthalene (97%, J&K), Benzil (99%, Innochem), Ethylene glycol (99%, Alfa), Polyphosphoric acid (84%, Alfa), Gallic acid hydrate (>98%, TCI), 1-Bromohexane (>98%, TCI), 1-Bromodecane (>98%, TCI), 1-Bromotetradecane (>97%, TCI) were used as received. All other chemical reagents were commercially available and used as received.

Measurements

^{1}H NMR spectra in solution were obtained from Bruker Avance 400 instruments. Multiplicities are denoted as follows: s = singlet, d = doublet, and m = multiplet. Fourier transform infrared spectra (FT-IR) were recorded on a NICOLET iS50 infrared spectrometer. Mass spectra was recorded on a LCMS-2020 single quadrupole equipped with an electrospray ionization (ESI) source interface (Shimadzu). Ultraviolet visible (UV-vis) spectra were recorded on a Shimadzu UV-2550 spectrometer. Fluorescence spectra were recorded with a Hitachi F-4600 FL Spectrophotometer. The absolute fluorescence quantum yield and time-resolved fluorescence lifetime experiments were performed with an Edinburgh FLS980 transient steady-state fluorescence spectrometer. Thermogravimetric analyses (TGA) were carried out on a Mettler Toledo TGA/DSC 1 system under nitrogen atmosphere at a flow rate of 15 mL min^{-1} with the scanning rate of 20 °C min^{-1} from 50 °C to 550 °C. Differential scanning calorimetry (DSC) thermograms were recorded on a Mettler Toledo DSC 1 system equipped with a cooling accessory and under nitrogen atmosphere at a flow rate of 20 mL min^{-1}. Typically, about 5 mg of the solid sample was encapsulated in a sealed aluminum pan with an identical empty pan as the reference with a heating or cooling rate of 10 °C min^{-1}. The polarized optical microscopy (POM) was adopted to characterize thermal transitions, observe and photograph textures with a Nikon E400POL microscope equipped with an INSTEC HCS302 hot and cold stage. X-ray scattering experiments were performed with a high-flux small-angle X-ray scattering instrument (SAXSess mc^2, Anton Paar) equipped with Kratky block-collimation system and a temperature control unit (Anton Paar TCS 120 and TCS 300). Both small angle X-ray scattering and wide angle X-ray scattering were simultaneously recorded on an imaging-plate (IP) which extended to high-angle range (the q range covered by the IP was from 0.06 to 29 nm^{-1}, $q = 4\pi\sin\theta/\lambda$, where the

wavelength λ is 0.1542 nm of Cu-Kα radiation and 2θ is the scattering angle) at 40 kV and 50 mA. The powder samples were encapsulated with aluminum foil during the measurement and the obtained X-ray analysis data were processed with the associated SAXSquant software 3.80 and the aluminum foil background signal was subtracted. Atomic force microscopy (AFM) images were obtained on a Bruker Dimension FastScan instrument. Samples were prepared by casting from chloroform solution on a cleaved silicon wafer.

2. Preparation of Hydrogen-Bonded Supramolecular Discotic Complexes

2.1. Synthesis of Various TIB Derivatives

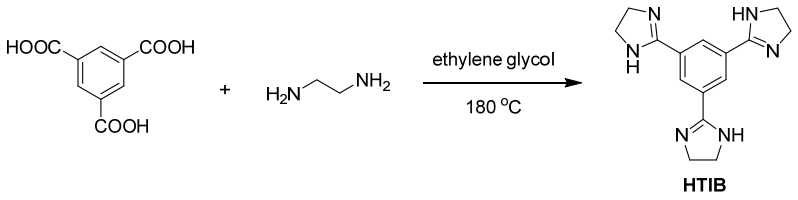

Scheme S1. Synthetic route of HTIB

1,3,5-tris(4,5-dihydro-1*H*-imidazol-2-yl)benzene (HTIB). The synthesis of HTIB was performed according to the literature procedure.[1] Yield 75%; White solid; M.P. >300 °C. ^{1}H NMR (400 MHz, CD_3OD): δ = 8.25 (s, 3H), 3.81 (s, 12H). ESI-MS (m/z): $[M+H]^+$ calcd for $C_{15}H_{19}N_6$, 283.17, found, 282.82; $[M+Na]^+$ calcd for $C_{15}H_{18}N_6Na$, 305.15, found, 304.80.

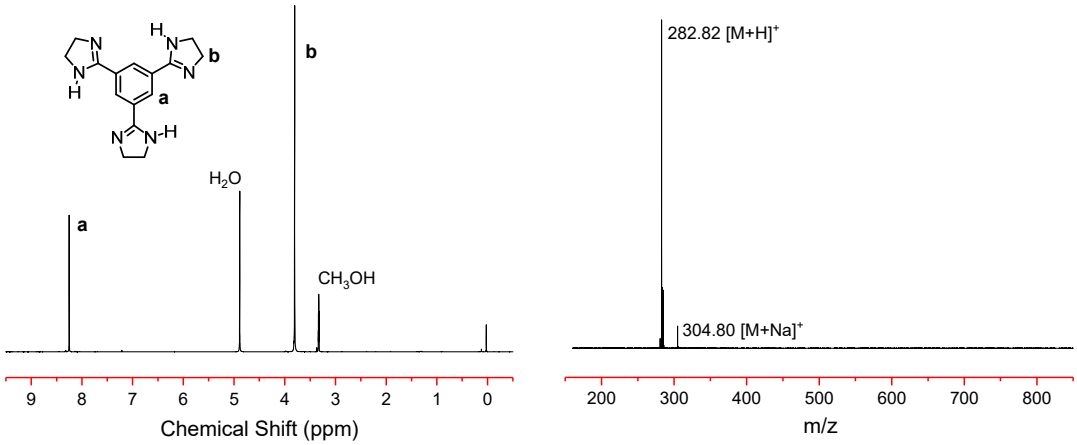

Figure S1. Molecular structure characterization for HTIB of ^{1}H NMR and ESI-MS spectra.

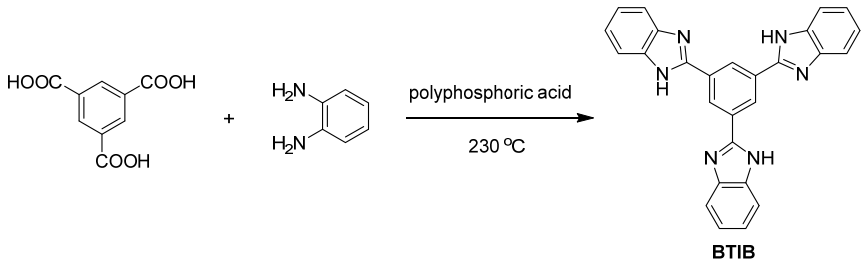

Scheme S2. Synthetic route of BTIB

1,3,5-tris(1*H*-benzo[*d*]imidazol-2-yl)benzene (BTIB). The synthesis of BTIB was performed according to the literature procedure.[2] Yield 70%; White solid; M.P. >300 °C. ^{1}H NMR (400 MHz, DMSO-d_6): δ = 13.38 (s, 3H), 9.12 (s, 3H), 7.78 (d, 3H, J = 7.2 Hz), 7.63 (d, 3H, J = 7.2 Hz), 7.29 (m, 6H). ESI-MS (m/z): $[M+H]^+$ calcd for $C_{27}H_{19}N_6$, 427.17, found, 426.88; $[M+Na]^+$ calcd for $C_{27}H_{18}N_6Na$, 449.15, found, 448.87.

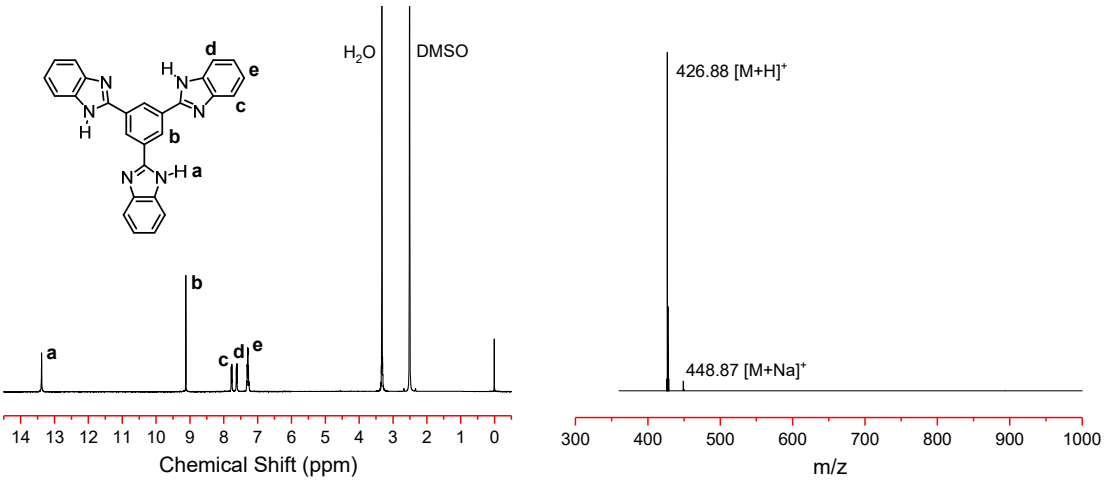

Figure S2. Molecular structure characterization for BTIB of ^{1}H NMR and ESI-MS spectra.

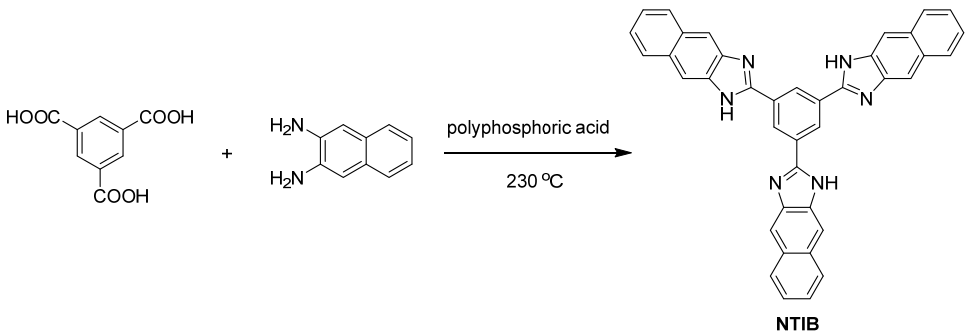

Scheme S3. Synthetic route of NTIB

1,3,5-tris(1*H*-naphtho[2,3-*d*]imidazol-2-yl)benzene (NTIB). The synthesis of NTIB was performed according to the procedure in preparing BTIB by using 2,3-diaminonaphthalene instead of 1,2-phenylenediamine as the starting material. Yield 80%; Dark brown solid; M.P. >300 °C. ^{1}H NMR (400 MHz, DMSO-d_6): δ = 13.53 (s, 3H), 9.39 (s, 3H), 8.36 (s, 3H), 8.13, 8.11, 8.08 (s, 9H), 7.44 (s, 6H). ESI-MS (m/z): $[M+H]^+$ calcd for $C_{39}H_{25}N_6$, 577.21, found, 577.03; $[M+Na]^+$ calcd for $C_{39}H_{24}N_6Na$, 599.20, found, 598.96.

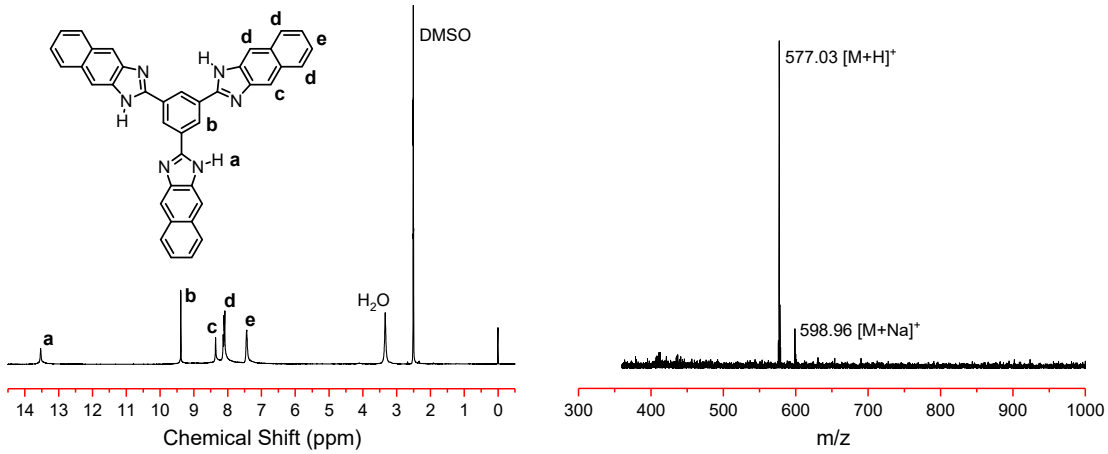

Figure S3. Molecular structure characterization for NTIB of ^{1}H NMR and ESI-MS spectra.

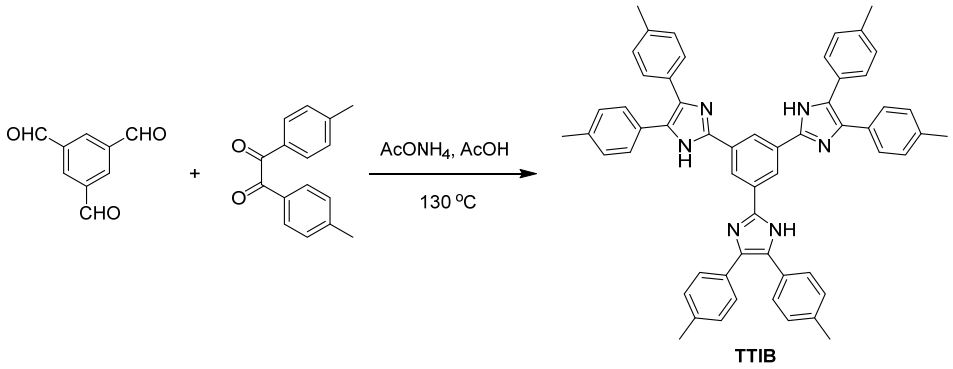

Scheme S4. Synthetic route of TTIB

1,3,5-tris(4,5-di-*p*-tolyl-1*H*-imidazol-2-yl)benzene (TTIB). The synthesis of TTIB was performed referring to the literature with some modifications.[3] A mixture of 1,3,5-triformylbenzene (300 mg, 1.85 mmol), 4,4'-dimethylbenzil (1.41 g, 5.93 mmol), and ammonium acetate (13.7 g, 177.8 mmol) in 12 mL acetic acid was refluxed at 130 °C overnight. The reaction mixture was allowed to cool to room temperature and was neutralized by aqueous ammonia. The crude product was washed with hot

methanol, to give a desired product. Yield 40%; White or pale yellow solid; M.P. >300 °C. ^{1}H NMR (400 MHz, DMSO-d_6): δ = 12.87 (s, 3H), 8.69 (s, 3H), 7.51 (d, 6H, J = 8.0 Hz), 7.44 (d, 6H, J = 8.0 Hz), 7.27 (d, 6H, J = 8.0 Hz), 7.15 (d, 6H, J = 8.0 Hz), 2.36, 2.31 (s, 18H). ESI-MS (m/z): $[M+H]^+$ calcd for $C_{57}H_{49}N_6$, 817.40, found, 817.37; $[M+Na]^+$ calcd for $C_{57}H_{48}N_6Na$, 839.38, found, 839.35; $[M+K]^+$ calcd for $C_{57}H_{48}N_6K$, 855.36, found, 855.33.

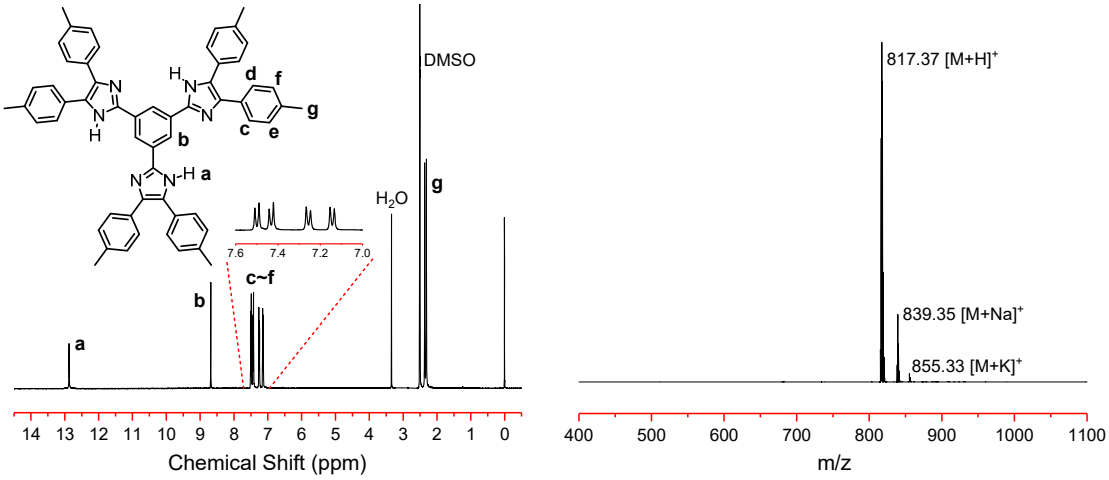

Figure S4. Molecular structure characterization for TTIB of ^{1}H NMR and ESI-MS spectra.

2.2. Synthesis of Carboxylic Acids A_n with Different Length Alkyl Tails

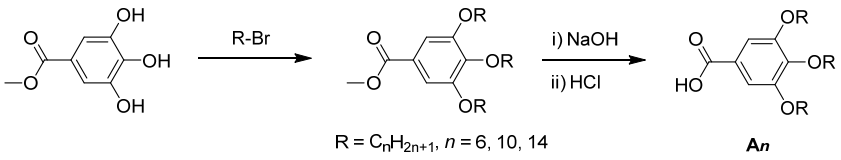

Scheme S5. Synthetic route of carboxylic acids A_n

The synthesis of A_n with different alkyl tails (n = 6, 10, 14) was according to the literature procedure.[2b] Taking methyl 3,4,5-trihydroxybenzoate as the starting material, first through Williamson etherification of phenolic hydroxyl groups with variant lengths n-alkyl bromide, and then hydrolysis of the methyl ester group, the 3,4,5-trialkyloxybenzoic acids A_n were finally obtained in a high yield. The typical characterization data of representative A_{10} were displayed as followed. White solid; M.P. 47 °C. ^{1}H NMR (400 MHz, $CDCl_3$): δ = 7.34 (s, 2H), 4.05 (m, 6H), 1.9-1.2 (m, 48H), 0.91 (t, 9H, J = 6.8 Hz). ESI-MS (m/z): $[M-OH]^+$ calcd for $C_{37}H_{65}O_4$, 573.49, found, 573.32;

$[M+Na]^+$ calcd for $C_{37}H_{66}O_5Na$, 613.48, found, 613.32.

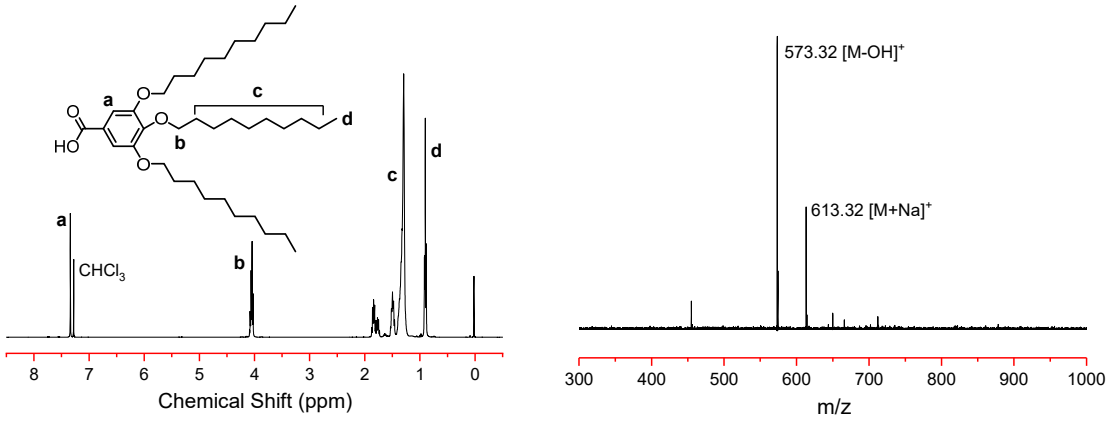

Figure S5. Molecular structure characterization for A_{10} of ^1H NMR and ESI-MS spectra.

2.3. Preparation of Supramolecular Complexes with Various TIB Templates and A_n

Two components of TIB compounds and A_n with a molar ratio of 1:3, respectively, were dissolved in chloroform. A small amount of methanol (for HTIB, BTIB and TTIB series) or dimethyl sulfoxide (for NTIB series) was then added to the solution to assist dissolution and formation of the supramolecular complexes. The resulting solution was allowed to reflux for several hours before solvent evaporation under reduced pressure. The obtained supramolecular discotic complex, TIB-A_n, was finally dried in vacuum overnight. The formation of supramolecular complexes was verified by ^1H NMR and FT-IR spectra analysis, and some of the typical characterization results for representative TIB-A_{10} were displayed as follows.

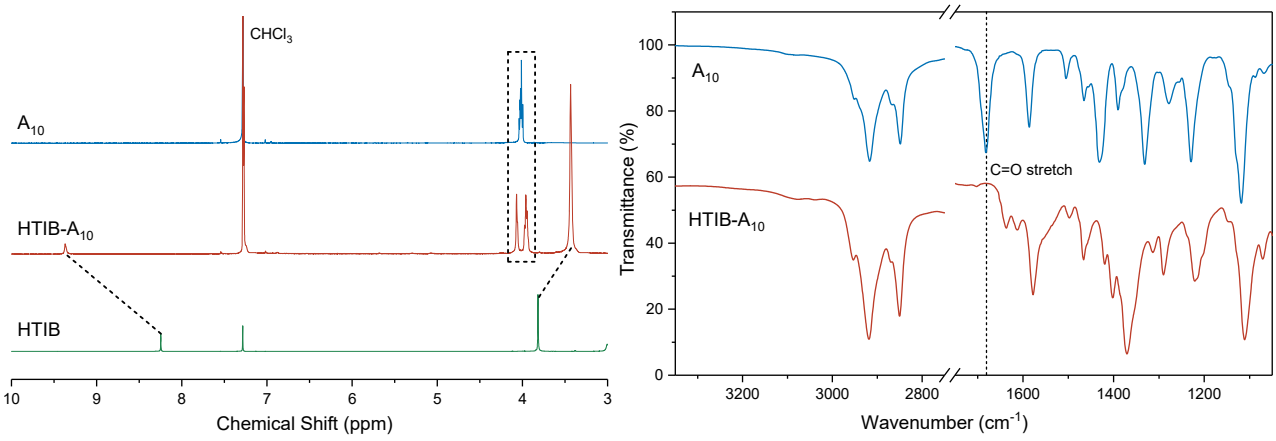

Figure S6. Comparison of ^1H NMR ($CDCl_3/CD_3OD$ = 24:1) and FT-IR spectra for identifying the formation of HTIB-A_{10} complex.

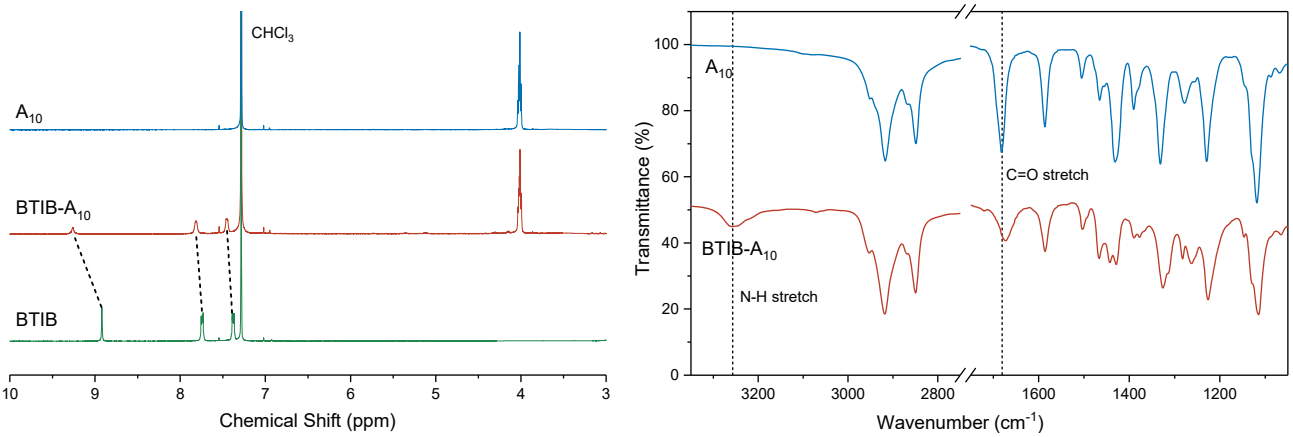

Figure S7. Comparison of ^{1}H NMR ($CDCl_3$/CD_3OD = 24:1) and FT-IR spectra for identifying the formation of BTIB-A_{10} complex.

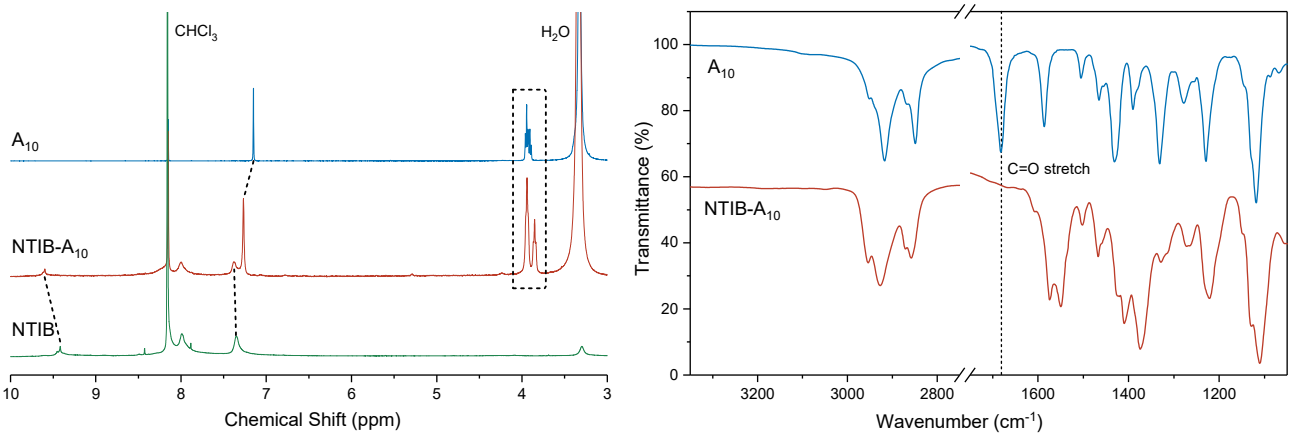

Figure S8. Comparison of ^{1}H NMR ($CDCl_3$/$(CD_3)_2SO$ = 5:2) and FT-IR spectra for identifying the formation of NTIB-A_{10} complex.

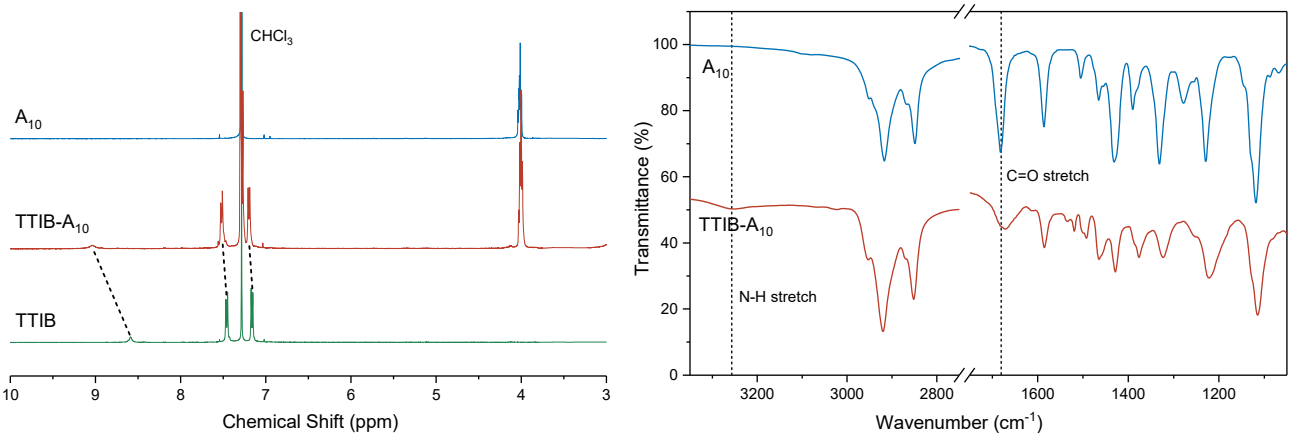

Figure S9. Comparison of ^{1}H NMR ($CDCl_3$/CD_3OD = 24:1) and FT-IR spectra for identifying the formation of TTIB-A_{10} complex.

Comparison of the NMR and IR spectra of the individual components with the corresponding complex was carried out to demonstrate the formation of hydrogen-bonded discotic supramolecular complexes (Figure S6-S9). The aromatic proton resonance peak of the central benzene unit of the TIB core shifted downfield after complexing with benzoic acid. This downshift of the proton resonance might result from the deshielding induced by the nearby dipole of the hydrogen-bonded carboxylic acid-imidazolyl pairs,[4] and thus gave some additional resonance signal variations (Figure S6-S9). Furthermore, the integral ratio of the characteristic ^{1}H NMR peak clearly indicated that the complexes were composed of corresponding TIB core and A_n in a given 1:3 molar ratio. The FT-IR absorption band of A_n at 1682 cm^{-1} was assigned to the C=O stretching vibration of dimeric hydrogen bonded carboxylic acids, which was lower than 1733 cm^{-1} of the free carboxylic acid.[4a,b] This absorption band was broadened and shifted to a wavelength of 1672 cm^{-1} after the complexation with BTIB and TTIB compounds (Figure S7,S9), as well as a pronounced band arose at 3260 cm^{-1} typical for the stretching vibration of hydrogen-bonded proton C=N…H-O between imidazolyl moiety and benzoic acid,[5] both of which suggested that the carbonyl group interacted with the imidazole in TIB and thus formed stronger hydrogen bond (Figure S10).[4b,5] However, in the case of HTIB-A_{10} and NTIB-A_{10}, there was no peak estimated as C=O peak after complex formation, which pointed to a different hydrogen-bonding mechanism. It is probably because the strong alkalinity of the HTIB that led to the formation of imidazolium carboxylate with A_{10}, between which the hydrogen bond took effect (Figure S10). This assumption was verified by the disappearance of the C=O peak of A_n at 1682 cm^{-1} replaced with a peak at 1637 cm^{-1} corresponding to $O=C=O^{-}$ stretching vibration after complex formation, as well as the disappearance of the C=N peak of HTIB at 1622 cm^{-1} (Figure S11). Moreover, the apparent ^{13}C NMR peak shift in Figure S11 might provide additional evidence for this special hydrogen-bonding mechanism. As for NTIB-A_{10}, a similar FT-IR pattern was obtained and compared with the NTIB and A_{10} components as illustrated in Figure S11, demonstrating the same interacting manner as HTIB-A_{10}. With these NMR and IR spectroscopy observations in hand, we may conclude the successful formation of hydrogen-bonded 1:3 discotic complexes TIB-A_n.

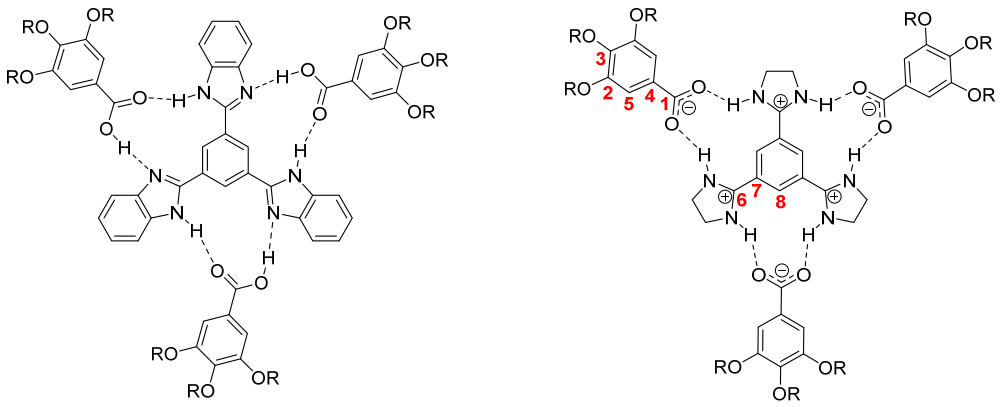

Figure S10. Proposed hydrogen-bonding manner for representative HTIB-A_{10} and NTIB-A_{10} complexes.

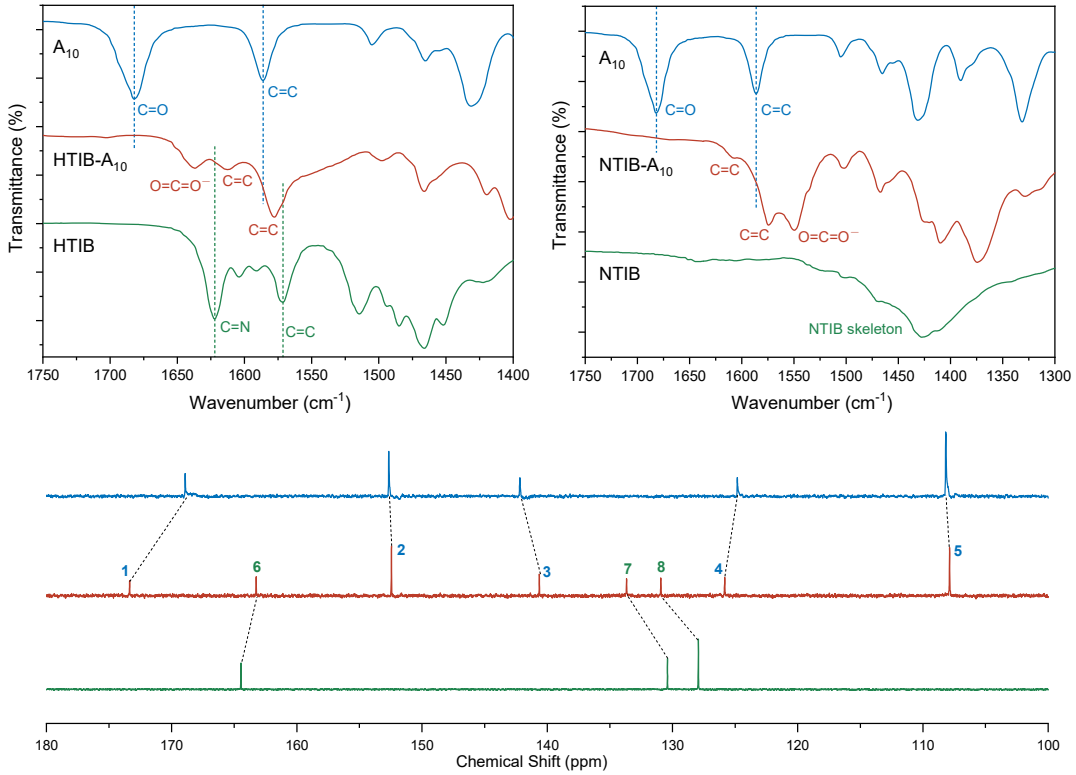

Figure S11. Enlarged FT-IR spectra for illustrating the hydrogen-bonding interactions for the formation of HTIB-A_{10} and NTIB-A_{10} complexes (top). ^{13}C NMR spectra comparison during the HTIB-A_{10} complex formation (down).

3. Thermal Characterization by TGA, DSC and POM

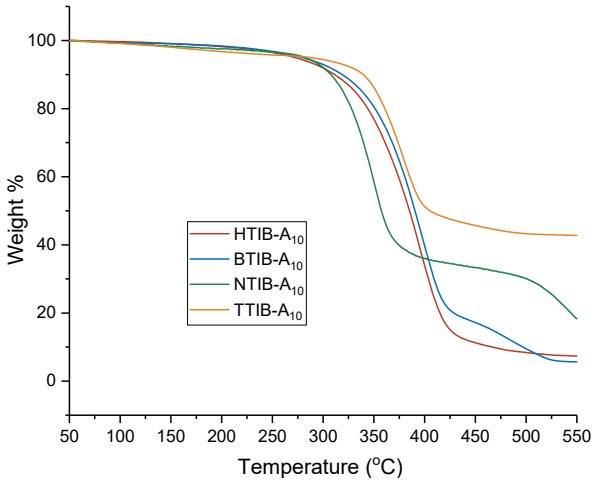

Figure S12. Representative TGA curves of TIB-A10 complexes.

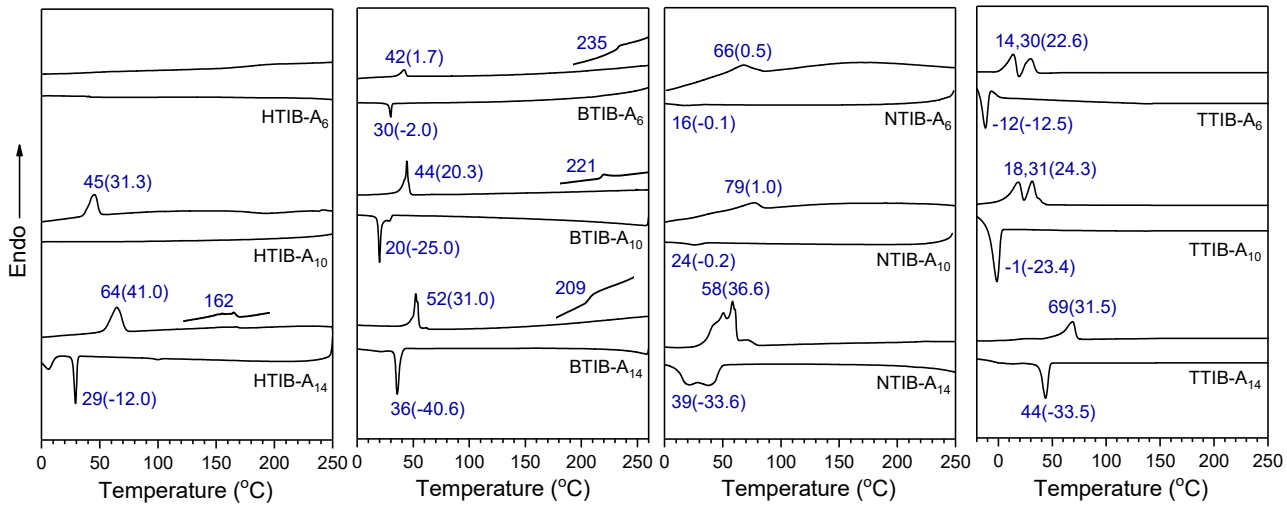

Figure S13. DSC heating and cooling traces of discotic TIB-A*n* complexes, indicating with transition peak temperatures (in °C), and associated enthalpy changes (in parentheses, in J g^{-1}).

The enthalpies for the clearing transition from the mesophase to isotropic liquid were usually much small for these supramolecular LCs,[2b,5] whereas some still were discernable in the DSC heating traces for HTIB- and BTIB-based complexes (Figure S11). The isotropization temperatures for other complexes were determined by POM and XRD analysis.

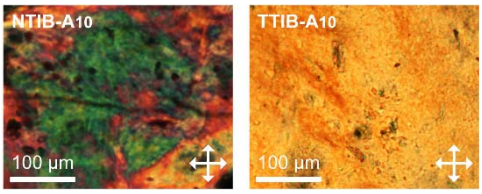

Figure S14. POM images of NTIB-A_{10} and TTIB-A_{10} sandwiched between two glass plates after mechanical pressing in their LC phases.

The POM images of complexes based on NTIB and TTIB (Figure S12) were collected from the samples by mechanical pressing in their LC phases, due to the unexpected occurrence of thermal decomposition before isotropization. After heating at temperatures larger than 250 °C for more than a few minutes, extended domains evolved which lacked birefringence and were surrounded by brown shades indicating decomposition of the textures.

4. Structural Analysis by XRD and Theoretical Simulation

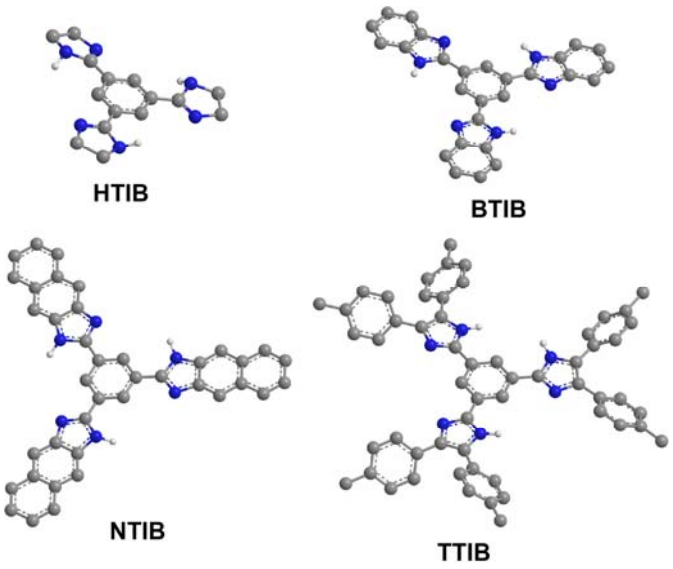

Figure S15. Optimized geometries of TIB compounds showing nearly planar HTIB but with a slight distortion in line with the reported crystallography characterization result,[6] almost planar BTIB and NTIB probably due to the π-expanded benzene or naphthalene fused rings, and twisted TTIB influenced by steric crowding of the outer six tolyl substituent groups.

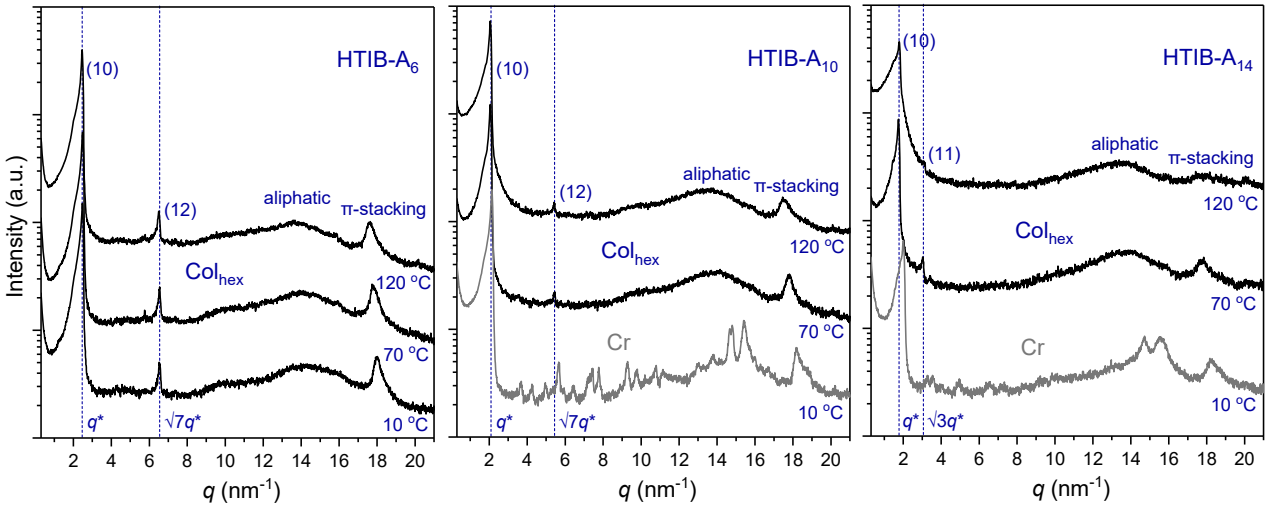

Figure S16. Variant temperature X-ray diffraction (XRD) patterns of discotic complexes HTIB-A$_n$ at indicated temperatures with proposed indexing and phase assignment.

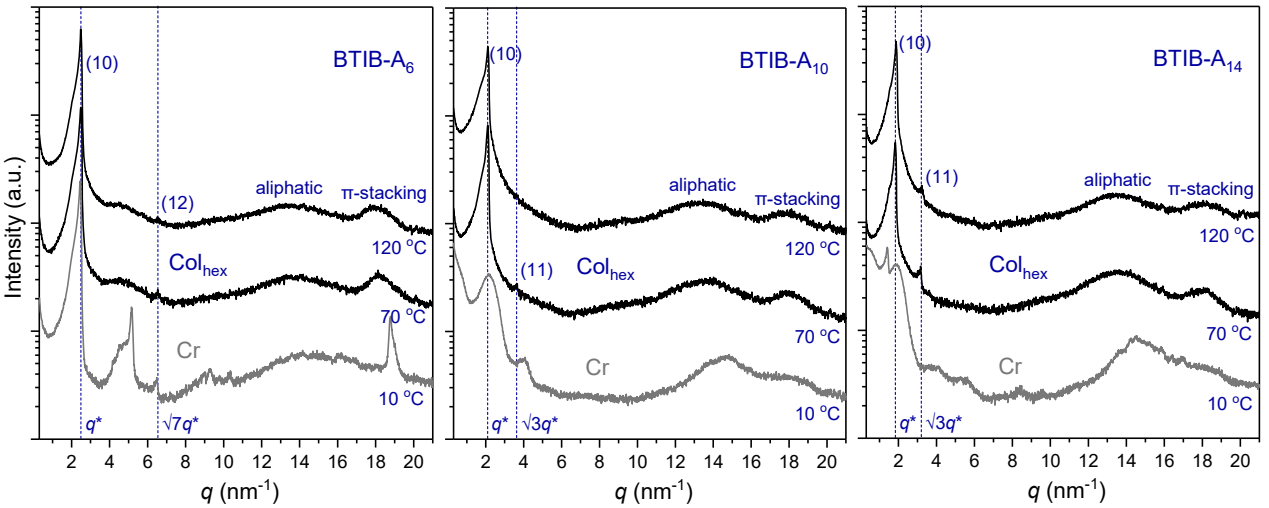

Figure S17. Variant temperature X-ray diffraction (XRD) patterns of discotic complexes BTIB-A$_n$ at indicated temperatures with proposed indexing and phase assignment.

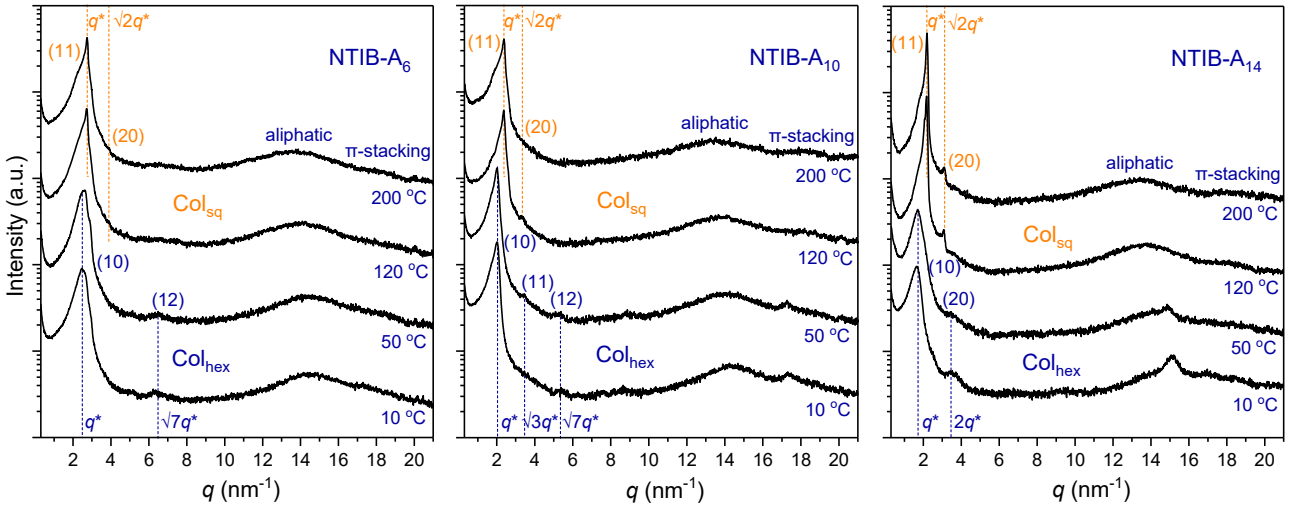

Figure S18. Variant temperature X-ray diffraction (XRD) patterns of discotic complexes NTIB-A$_n$ at indicated temperatures with proposed indexing and phase assignment.

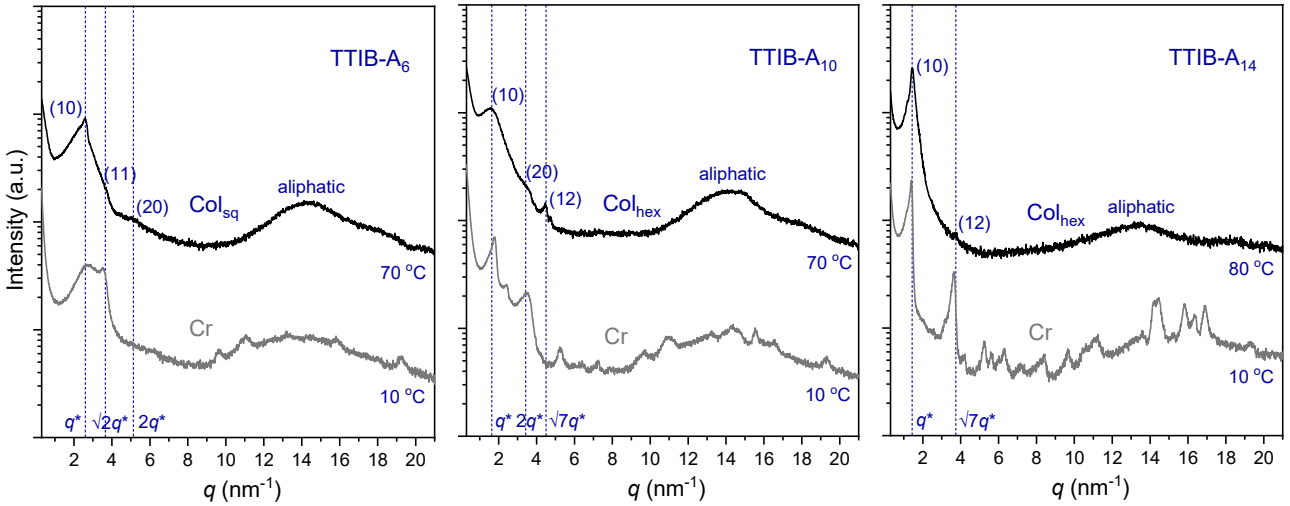

Figure S19. Variant temperature X-ray diffraction (XRD) patterns of discotic complexes TTIB-A$_n$ at indicated temperatures with proposed indexing and phase assignment.

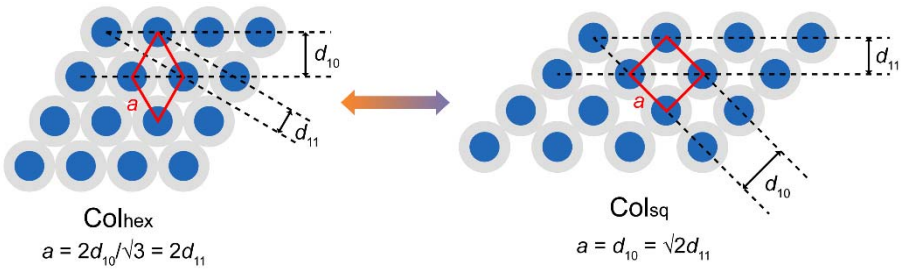

Figure S20. Schematic illustration of LC phase transition between hexagonal columnar (Col$_{hex}$) and square columnar (Col$_{sq}$) mesophases.

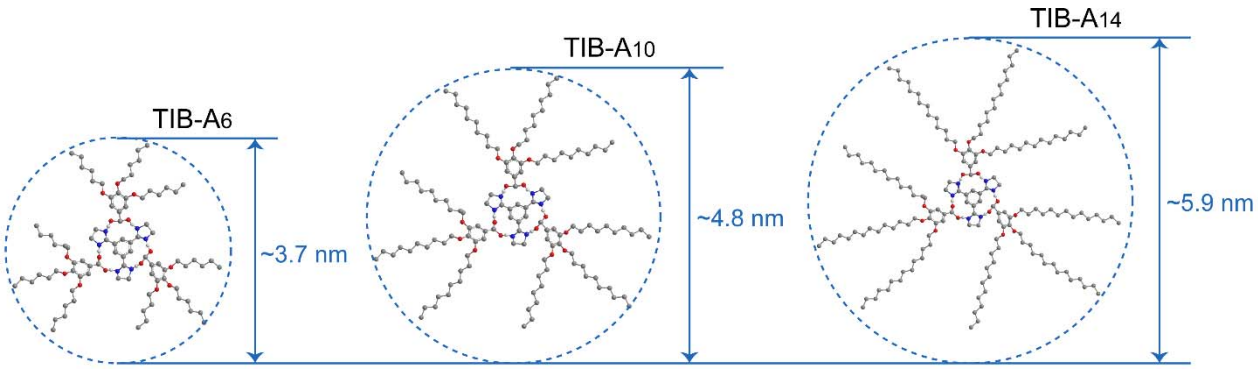

Figure S21. The estimated dimensions of discotic complexes TIB-A$_n$ in an extended conformation.

Table S1. Lattice parameter in LC mesophases of these hydrogen-bonded discotic TIB-A$_n$ complexes obtained from XRD analysis.

Components	HTIB-	BTIB-	NTIB-		TTIB-
	70 °C	70 °C	70 °C	120 °C	70/80 °C
-A$_6$	Col_{hex} (*p6mm*)	Col_{hex} (*p6mm*)	Col_{hex} (*p6mm*)	Col_{sq} (*p4mm*)	Col_{sq} (*p4mm*)
	a = 2.92 nm	*a* = 2.92 nm	*a* = 2.95 nm	*a* = 3.22 nm	*a* = 3.43 nm
	c = 0.35 nm	*c* = 0.35 nm	*c* = 0.36 nm	*c* = ~0.35 nm	*c* = ~0.35 nm
-A$_{10}$	Col_{hex} (*p6mm*)	Col_{hex} (*p6mm*)	Col_{hex} (*p6mm*)	Col_{sq} (*p4mm*)	Col_{hex} (*p6mm*)
	a = 3.52 nm	*a* = 3.47 nm	*a* = 3.68 nm	*a* = 3.72 nm	*a* = 4.29 nm
	c = 0.35 nm	*c* = 0.35 nm	*c* = 0.36 nm	*c* = ~0.35 nm	*c* = ~0.35 nm
-A$_{14}$	Col_{hex} (*p6mm*)	Col_{hex} (*p6mm*)	Col_{hex} (*p6mm*)	Col_{sq} (*p4mm*)	Col_{hex} (*p6mm*)
	a = 4.14 nm	*a* = 4.06 nm	*a* = 4.32 nm	*a* = 4.15 nm	*a* = 5.14 nm
	c = 0.35 nm	*c* = 0.35 nm	*c* = ~0.36 nm	*c* = ~0.35 nm	*c* = ~0.35 nm

5. Additional Spectroscopy Data

Table S2. Spectroscopy data of these hydrogen-bonded complexes based on different TIB cores obtained from dilute chloroform solution or solid state.

		HTIB-A_{10}	BTIB-A_{10}	NTIB-A_{10}	TTIB-A_{10}
Dilute Solution	Absorption (nm)	261	311	273, 345	301, 330
	Emission (nm)	343	381	460	413
Solid State	Absorption (nm)	261	306	265	304
	Emission (nm)	361	511	355, 438	561

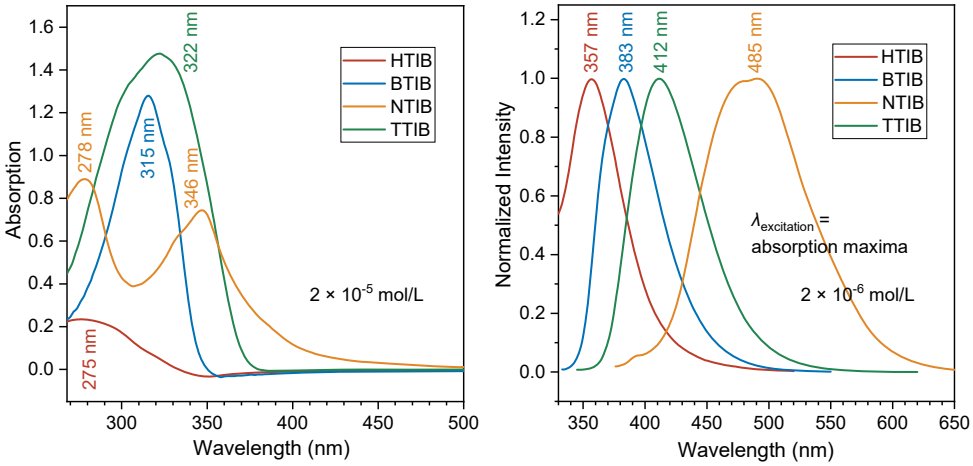

Figure S22. UV-vis absorption and fluorescence emission spectra of neat TIB compounds in dimethyl sulfoxide (DMSO) solution.

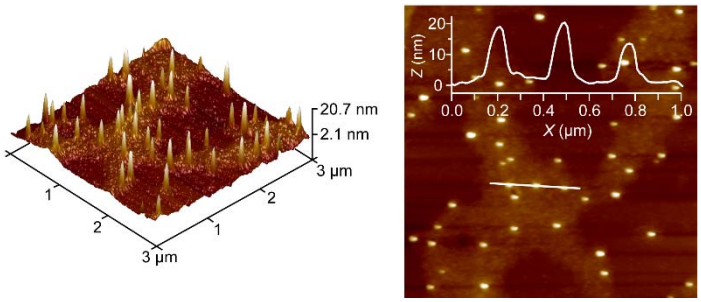

Figure S23. Atomic force microscopy (AFM) images obtained from 2×10^{-3} mol L^{-1} chloroform solution of TTIB-A_{10}, exhibiting irregular nanoaggregates.

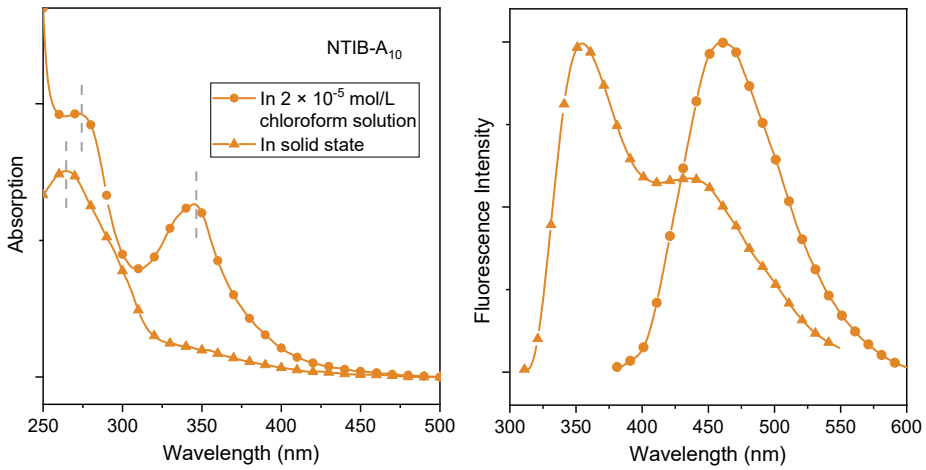

Figure S24. Comparison study of UV-vis absorption and fluorescence emission spectra obtained from TIB-A_{10} complex in 2 × 10^{-5} mol L^{-1} chloroform solution or solid state.

6. Supplementary References

1 (a) A. Kraft and F. Osterod, *J. Chem. Soc., Perkin Trans. 1.,* 1998, 1019-1026; (b) H. Yang, Z. M. Chen, J. J. Sun, S. P. Yang, J. Yu, H. Tan and W. Li, *Dalton Trans.,* 2009, 2540-2551.

2 (a) N. Chandrashekhar, B. Thomas, V. Gayathri, K. V. Ramanathan, N. Gowda, *Magn. Reson. Chem.,* 2008, **46,** 769-774; (b) J. F. Xiong, S. H. Luo, J. P. Huo, J. Y. Liu, S. X. Chen and Z. Y. Wang, *J. Org. Chem.,* 2014, **79,** 8366-8373.

3 (a) S. Hatano and J. Abe, *J. Phys. Chem. A,* 2008, **112,** 6098-6103; (b) K. Mutoh, Y. Kobayashi, T. Yamane, T. Ikezawa and J. Abe, *J. Am. Chem. Soc.,* 2017, **139,** 4452-4461.

4 (a) M. H. Ryu, J. W. Choi, H. J. Kim, N. Park and B. K. Cho, *Angew. Chem. Int. Ed.,* 2011, **50,** 5737-5740; (b) P. Xing, S. Z. F. Phua, X. Wei and Y. Zhao, *Adv. Mater.,* 2018, **30,** 1805175; (c) A. Kraft, *J. Chem. Soc., Perkin Trans. 1,* 1999, 705-714.

5 (a) G. M. Bögels, J. A. M. Lugger, O. J. G. M. Goor and R. P. Sijbesma, *Adv. Funct. Mater.,* 2016, **26,** 8023-8030; (b) J. A. M. Lugger, D. J. Mulder, S. Bhattacharjee and R. P. Sijbesma, *ACS Nano,* 2018, **12,** 6714-6724.

6 (a) A. Kraft and R. Fröhlich, *Chem. Commun.,* 1998, 1085-1086; (b) Y. B. R. D. Rajesh, S. Ranganathan, R. D. Gilardi abd I. L. Karle, *J. Chem. Crystallog.,* 2008, **38,** 39-48; (c) S. R. Nam, H. Y. Lee and J. I. Hong, *Tetrahedron,* 2008, **64,** 10531-10537.